A Passive Propellant Feeding Mechanism for Micropropulsion Using Capillarity

Kurt A. Polzin* **and Edgar Y. Choueiri†**
Electric Propulsion and Plasma Dynamics Laboratory (EPPDyL)
Mechanical and Aerospace Engineering Department
Princeton University, Princeton, New Jersey 08544

AIAA-2002-3949‡

July 7-10, 2002

The idea of using capillarity as a mechanism to passively control the propellant flow in microthrusters is explored. A capillary tube consisting of two different radius sections can be employed to passively 'pump' a fluid within the tube and keep a microthruster continuously supplied with propellant. A simple, one-dimensional fluid model is developed and tested using five different fluids and five different combinations of larger and smaller radius tube sections. Non-dimensional similarity parameters are derived from the theoretical fluid model, and used to transform the dimensional experimental data from a set spanning four orders of magnitude to a set falling within one order of magnitude of the one-dimensional theory. A gravitational correction, based on physical arguments, enables the theoretical model and data set to more closely agree. The resulting experimentally verified scaling laws provide the fundamental tools for designing passive capillary mass feeding systems for micropropulsion.

I. INTRODUCTION

There is presently a strong interest in developing micropropulsion systems for spacecraft. This motivation springs from two different types of applications: 1) microspacecraft, which have low power levels available and require low mass thrusters, and 2) the fine positioning of spacecraft constellations for missions such as interferometric observatories[1, 2], where low thrust levels and fine thrust resolution are required. Many of the current thruster options currently being considered for micropropulsion use are reviewed by Mueller[3].

Apart from the challenges associated with the development of microthrusters that are lightweight and use very low levels of power, there are challenging issues with propellant storage and handling. Gas propellant storage can carry a high tankage mass penalty and the valves currently under development to control liquid and gaseous propellants have high leak rates[4].

An alternative to high pressure gas or volatile liquid propellants may exist. A low vapor pressure, liquid propellant flow could be passively controlled to feed a thruster by capillary action, thus eliminating the need for valves. We will show that the propellant flow rate can be controlled by tailoring the capillary tube geometry. This scheme could be used to feed propellant to a microthruster, or propellant could simply be ejected from the end of the tube by a proper expulsion scheme[1], as illustrated in Fig. 1.

II. MICROFLUIDICS

Currently, there is much research and development work on actuators, pumps, flow sensors and

*Graduate Research Assistant. National Defense Science and Engineering Graduate Fellow. Member AIAA.

†Chief Scientist at EPPDyL. Associate Professor, Applied Physics Group. Associate Fellow AIAA.

‡Presented at the 38^{th} AIAA/ASME/SAE/ASEE Joint Propulsion Conference, Indianapolis, IN, July 7-10, 2002.

[1] The evaluation of ink-jet technologies[5] for this purpose is currently underway.

flow controllers, which make use of microfluidic flows. Many of these applications are reviewed in Shoji and Esashi[6] and Elwenspoek *et al*.[7] Also, there have been several fundamental studies dealing with how fluids advance in capillaries, specifically how the contact angle forms and changes as the interface (meniscus) moves[8–12] or how to control and model fluid flows on a small scale[13, 14] for, among other applications, integrated lab-on-a-chip devices[15, 16].

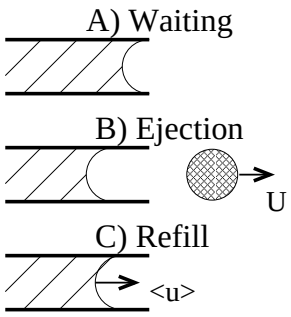

FIG. 1: A sequence showing how a thrust-on-demand device, using capillarity for propellant control, would work.

Most of the studies mentioned above rely on either active flow control (i.e. pistons, pressurized gases, pumps, temperature profiles) or gravity acting on a column of fluid to force it through a capillary or small channel. Having moving parts like pistons or valves for pressurization in a microsat is undesirable due to the added size, weight and complexity these devices entail.

Luckily, there exists a geometric prescription that will yield a net force on a fluid and cause it to move without any outside intervention. However, the microfluidics of such a scheme have not been systematically investigated.

A capillary tube possessing a different radius at each end (with the radius either changing through a continuous taper or a discontinuous step) will produce a net force acting on the fluid[17]. Just as importantly, when the fluid reaches the end of the tube, it will not leave the tube because the meniscus must turn from concave to convex for the fluid to exit, and the same force which drove the fluid to the end of the tube prevents this from happening. Finally, fluid that is ejected from the end of the capillary is replaced by the same capillary mechanism. Developing an understanding of free, passive capillary flows will allow us to develop relations which could then be used to scale and optimize microthruster performance parameters like the mass flow rate.

It is worth noting that this type of capillary flow is implicitly at play in Field Emission Electric Propulsion (FEEP) thrusters[18]. However, the mass flow rates in these devices are limited by the amount of field ionization to tiny amounts, so it has never been necessary to model or optimize the capillary flows in these devices.

The remainder of this paper will be organized as follows. In section III, a theoretical fluid model of passive capillary flows will be developed. Section IV is divided into three subsections. Section IV A contains a description of the experimental apparatus used to explore and rigorously test the theoretical model. In section IV B, the experimental results are presented. Finally, a set of scaling laws are derived and applied to the experimental data set in section IV C.

III. FLUID MODEL

In this section, we develop a simple, one-dimensional model of a fluid flow in a stepped capillary tube (i.e. a tube with two constant-radius sections meeting in a discontinuous step)(see Fig. 2). This model will later be used to non-dimensionalize experimental data and determine similarity parameters for flows of this type.

Neglecting inertia, time variations, and gravity, the Navier-Stokes equation can be written as

$$0 = -\nabla P + \eta \nabla^2 u, \tag{1}$$

where P is the pressure, η is the viscosity coefficient and u is the fluid velocity. This equation is solved using the boundary conditions

$$u\left(R\right) = 0, \quad u\left(0\right) \text{ bounded}, \tag{2}$$

where R is the capillary tube radius. Assuming that u varies only in the radial direction and dP/dx is equal to a constant k, the solution to Eq. (1) is the

laminar, parabolic velocity profile

$$u(r) = \frac{k}{4\eta}\left(R^2 - r^2\right). \tag{3}$$

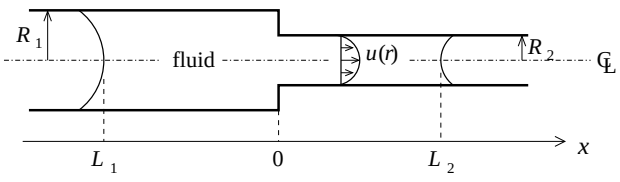

FIG. 2: Schematic of the capillary tubes.

We define the average velocity as

$$\langle u \rangle = \frac{\int_0^{2\pi}\int_0^R u(r)\, r\, dr\, d\theta}{\pi R^2} = \frac{kR^2}{8\eta} \tag{4}$$

This is the well-known Poiseuille flow solution for laminar flow in a pipe[19]. The pressure within each tube of constant radius changes linearly due to the viscosity, yielding a constant pressure gradient, k, for each tube. Using Eq. (4) in the incompressible continuity equation ($\langle u \rangle A$ = a constant) gives the compatibility condition

$$k_1 = \left(\frac{R_2}{R_1}\right)^4 k_2, \tag{5}$$

where the subscripts 1 and 2 refer to the larger and smaller radius tubes, respectively.

We introduce a closure assumption for this formulation in the form of a pressure profile. The meniscus at each end of the tube is exposed to the same outside pressure (see Fig. 3). At each meniscus there will be a jump discontinuity in the pressure. These discontinuities can be written in terms of the surface tension, σ, and wetting angle, θ, as

$$\Delta P_1 = \frac{2\sigma}{R_1}\cos\theta_1, \quad \Delta P_2 = \frac{2\sigma}{R_2}\cos\theta_2. \tag{6}$$

If the assumption of a fully-wetting fluid is employed (i.e. $\theta_1 = \theta_2 = 0$), we see that, for $R_2 < R_1$, ΔP_2 will always be greater than ΔP_1.

Using Eqs. (5) and (6) and assuming the pressure is piecewise continuous between the menisci (see Fig. 3), analytic expressions for k_1 and k_2, given values of the fluid column lengths, L_1 and L_2, and the tube radii, R_1 and R_2, can be found. These are

$$\begin{aligned} k_1 &= \frac{2\sigma\left(1/R_2 - 1/R_1\right)}{L_2 - L_1\left(R_2/R_1\right)^4}\left(R_2/R_1\right)^4 \\ k_2 &= \frac{2\sigma\left(1/R_2 - 1/R_1\right)}{L_2 - L_1\left(R_2/R_1\right)^4} \end{aligned} \tag{7}$$

Note from the coordinate system that L_1 is measured such that it is always negative, so the denominator is always positive. We can now compute theoretical values for $\langle u \rangle$ using Eq. (4).

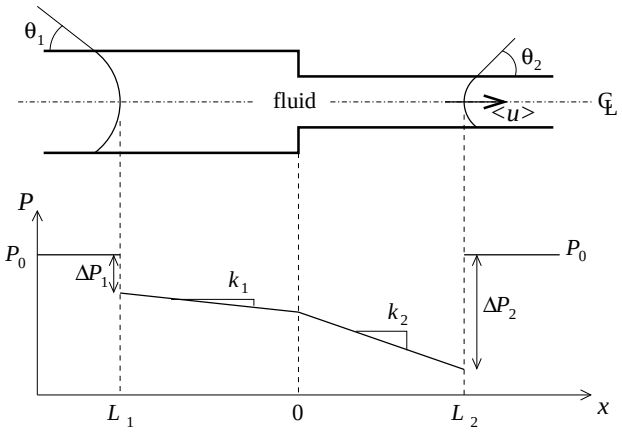

FIG. 3: Pressure profile in the fluid.

It is worth noting that the quantity L_{eq}, defined as

$$L_{eq} \equiv L_2 - L_1\left(R_2/R_1\right)^4, \tag{8}$$

has a physical interpretation. It is the length of a column of fluid having radius R_2 and constant pressure gradient, k_2, such that its pressure drop is equal to the pressure drops of the fluid columns with lengths L_1 and L_2. In other words, $|k_2 L_{eq}| = |k_1 L_1| + |k_2 L_2|$.

IV. CAPILLARY EXPERIMENTS

We would like to perform experiments that will allow us to verify the theoretical model developed in the previous section and develop the physical insight necessary to obtain relevant scaling relations. To do this, we have constructed stepped capillary tubes having different combinations of values of R_1 and R_2 and measured the velocity of the meniscus as it propagates into the smaller radius tube.

A. Experimental Apparatus

The experimental apparatus shown in Figs. 4 and 5 was used to test the fluid model developed above. Fluids were initially injected into the larger radius tube (right tube of Fig. 5) until the meniscus reached the smaller radius tube. Once the fluid entered the smaller radius tube, all active injection was halted.

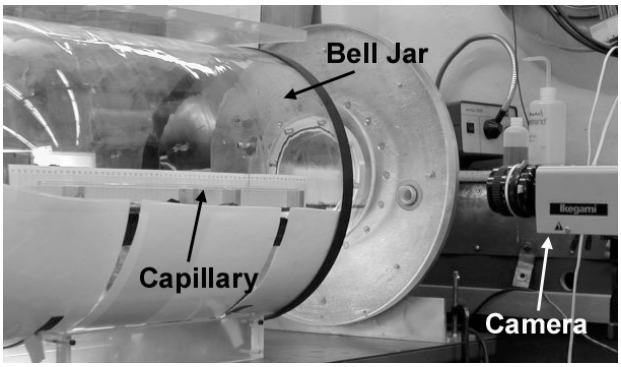

FIG. 4: Experimental set-up.

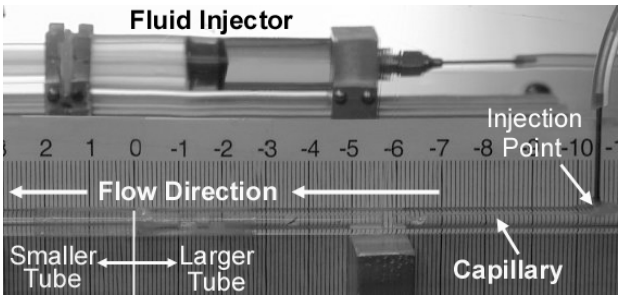

FIG. 5: Close up of the capillary tubes and fluid injection system.

The meniscus position was recorded onto videotape using a camera and VCR. We will present data which will give the velocity, $\langle u_2 \rangle$, as a function of meniscus position, L_2. It is obvious that at any particular instant in time, $\langle u \rangle$ along the length of a constant-area tube will be constant since these fluids are incompressible. To determine $\langle u_2 \rangle$, several meniscus positions centered around a given position, L_2, were recorded and a standard central difference was employed, yielding a measure of $\Delta x/\Delta t \approx \langle u_2 \rangle$. The measure of Δt was taken as the inverse of the framing rate of a standard VCR, which is equal to 29.97 Hz[20].

TABLE I: Different capillary tube radius combinations.

R_1 [mm]	R_2 [mm]
1.50	1.10
1.50	0.60
1.50	0.30
1.35	0.60
1.35	0.30

Five different capillary tube radius combinations were tested. These combinations are listed in Table I. In addition to varying the radii, five different fluids were tested. These were methanol, propanol-2 (iso-propyl alcohol), dibutyl phthalate, mechanical pump oil and diffusion pump oil. The last two fluids were chosen for their low vapor pressure, which underlines their suitability for operation in vacuum. The density (ρ), surface tension (σ), viscosity (η) and vapor pressure (P_v) of each fluid are listed in Table II. All properties for methanol and propanol were taken from Ref. [21]. The properties for dibutyl-phthalate, mechanical pump oil and diffusion pump oil, with the exception or σ, were taken from manufacturer data (Ref. [22] for dibutyl-phthalate, Ref. [23] for mechanical and diffusion pump oil).

The surface tensions and static wetting angles of dibutyl phthalate, mechanical pump oil and diffusion pump oil were measured by placing different tubes into a pool of the given liquid and recording the capillary-induced height rise, Δh, and the wetting angle. The surface tension can be calculated as[24]

$$\sigma = \frac{\rho g \Delta h r}{2 \cos \theta}. \tag{9}$$

Using this relation and a measured wetting angle of $\approx 60^o$, we obtained values for the surface tensions of dibutyl phthalate and diffusion pump oil which, within the data scatter, match the manufacturer's specifications of 34 and 33.9 mN/m, respectively.

TABLE II: Properties of fluids tested.

Name	ρ [kg/m^3]	σ [mN/m]	η [mPa-s]	P_v [Torr]
Methanol (CH_4O)	790	22.1	0.54	127
Propanol-2 (C_3H_8O)	835	20.9	2.04	45
Dibutyl Phthalate ($C_{16}H_{22}O_4$)	1044	16 (± 2.8)	20.3	0.72
Fisherbrand 19 mechanical pump oil	870	14 (± 2.9)	47.9	10^{-5}
Invoil 940 Si-diffusion pump oil	1070	16 (± 3.4)	25.9	10^{-8}

While the wetting angle will actually change as the fluid advances, these three fluids (dibutyl phthalate, mechanical pump oil and diffusion pump oil) are very viscous and will most likely advance slowly. In light of this, it seems reasonable to assume the contact angle during motion will not, for the most part, vary much from the static contact angle. The values of σ in Table II have been calculated assuming that the contact angle is zero (fully wetting). Note that this assumption can be justified by an inspection of the equation for the measured surface tension, Eq. (9), and the pressure drop across a meniscus, Eqs. (6). If the contact angle in each equation is essentially the same, the contact angles ($\cos\theta$ terms) cancel.

B. Experimental Results

The measured meniscus velocity as a function of meniscus position is presented in Figs. 6A and B. The data in Fig. 6A are for a large radius, R_1, of 1.35 mm, while the data in Fig. 6B are for $R_1 = 1.50$ mm. Several general trends are evident from these plots. The first is that the data spans more than 3 orders of magnitude in $\langle u_2 \rangle$. The second is that the meniscus moves more swiftly when R_2 is smaller. Also, the velocity appears to exhibit a functional dependence with L_2 which becomes steeper as R_2 increases.

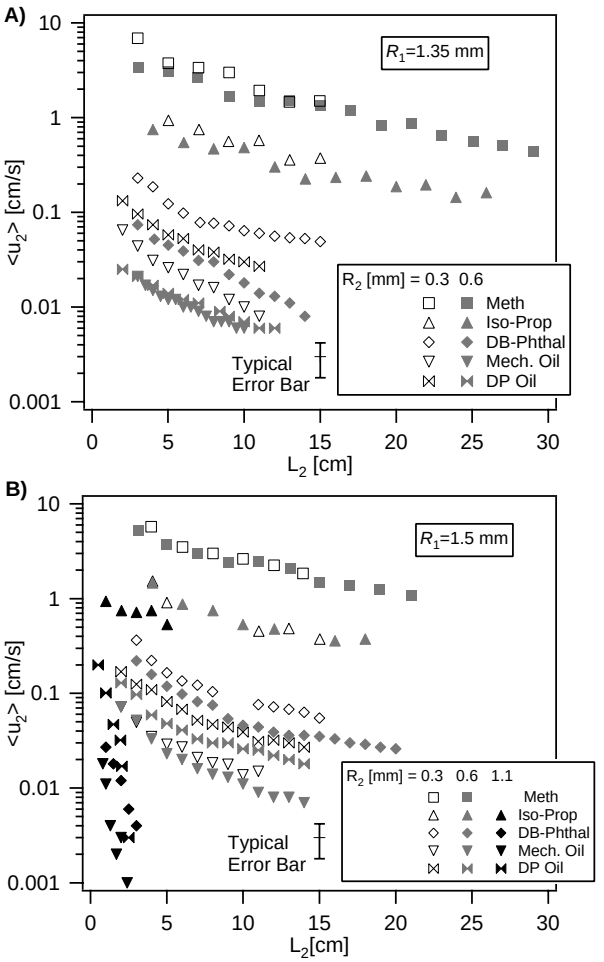

FIG. 6: Measured velocity as a function of meniscus position, L_2.

C. Fundamental Scaling Laws

Our goal now is to attempt to collapse these data onto a plot as a single, non-dimensional line. At this point, we introduce two dimensionless parameters relevant in the study of slow capillary flows. The Capillary number, Ca, and the Bond number, Bo, are defined as

$$\text{Ca} \equiv \frac{\eta \langle u \rangle}{\sigma} = \frac{\text{viscosity}}{\text{surface tension}},$$
$$\text{Bo} \equiv \frac{\rho g d^2}{\sigma} = \frac{\text{gravity}}{\text{surface tension}}, \qquad (10)$$

where d is the tube diameter and ρ is the fluid density.

Returning to the theoretical model for insight, we write out the meniscus front velocity explicitly by inserting Eq. (7) into Eq. (4) to obtain

$$\langle u_2 \rangle = \frac{R_2^2}{8\eta} \frac{2\sigma \left(1/R_2 - 1/R_1\right)}{L_{eq}}. \qquad (11)$$

This expression can be rearranged into the non-dimensional form

$$\frac{\langle u_2 \rangle \eta}{\sigma} \frac{1}{(1 - R_2/R_1)} = \frac{\mathrm{Ca}}{\zeta} = \frac{1}{8} \left(\frac{L_{eq}}{d_2} \right)^{-1}, \qquad (12)$$

where $\zeta = (1 - R_2/R_1)$ and $d_2 = 2R_2$. From this equation, we can define two new similarity parameters,

$$\Pi \equiv \frac{\mathrm{Ca}}{\zeta}, \quad \xi \equiv \left(\frac{L_{eq}}{d_2} \right). \qquad (13)$$

We refer to these as the free capillary flow parameter, Π and free capillary length, ξ. We note that Π is a combination of fluid properties (through Ca) and geometric properties (through ζ), while ξ contains the remaining geometric parameters.

The function in Eq. (12) is plotted as a solid line in Fig. 7 for a stepped capillary tube having a constant volume of fluid. In addition, we have taken all the velocity and position data found in Figs. 6A and B, converted them to the dimensionless parameters specified in Eqs. (13), and replotted these data in Fig. 7. We note here that the values of L_2 and L_{eq} are quite similar due to the scaling of L_1 by the factor $(R_2/R_1)^4$ in Eq. (8), which is a small number.

Figure 7 shows that the data has generally collapsed to within one order of magnitude in the ordinate with the introduction of the non-dimensional parameters, Π and ξ. Moreover, we notice a trend in this plot. For smaller leading menisci Bond numbers, Bo_2, the agreement with the theoretical model is good, while for larger values of Bo_2 the agreement deteriorates.

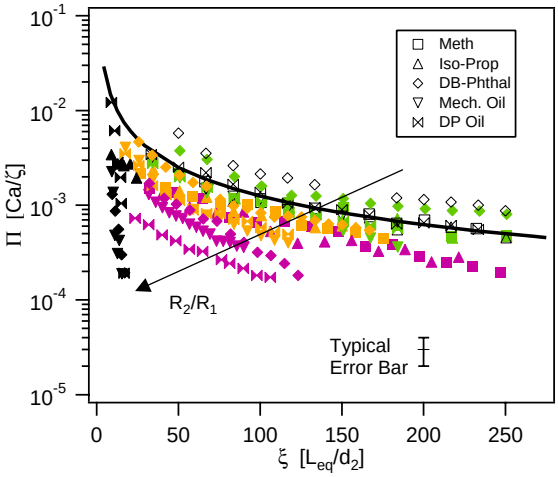

FIG. 7: A plot of all data in Figs. 6A and B. The data is plotted as the non-dimensional free capillary flow parameter as a function of non-dimensional length. The arrow is in the direction of increasing R_2/R_1. The line is the function in Eq. (12).

This can be understood in part through visual observations of the meniscus shape as a function of tube diameter. As the tube diameter increases (see Fig. 8), the meniscus deforms under the action of gravity. This deformation effectively increases the radius of curvature of the meniscus. Increasing the radius of curvature changes the pressure jumps at the leading and trailing menisci and results in an altered pressure profile within the fluid (see Eqs. (6)). This will cause the scaling parameter, Π, to deviate from its theoretical value through the deviation of the measured velocity, $\langle u_2 \rangle$, relative to the theory.

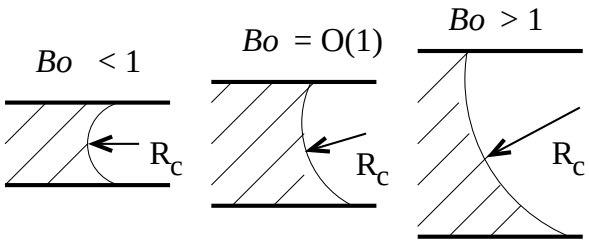

FIG. 8: A schematic showing how the meniscus shape varies with increasing Bond number.

Taking account of this effect requires extending the theory to 2-D at the price of significant analytical

complexity. Instead, we choose to find a correction to the 1-D theory that phenomenologically takes into account the complexity.

Gravitational correction: In an attempt to deal with this Bond number scaling, we seek a simple, first-order scaling relation that will effectively account for this increase in radius of curvature and yield a small correction. It is convenient to define a reference condition, where the gravitational effect is small. We define our reference as the case where methanol is flowing in a capillary tube having a radius of 0.3 mm.

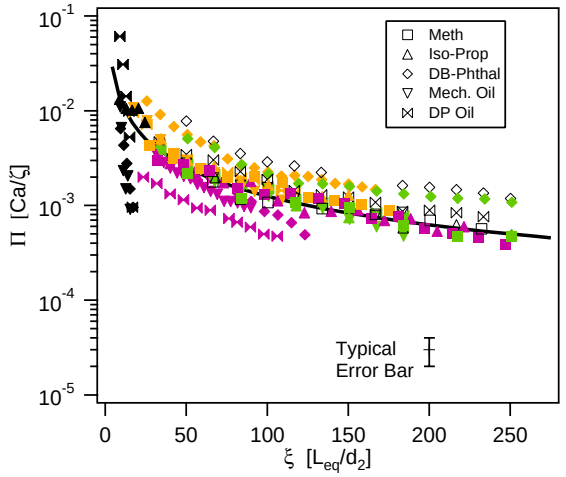

FIG. 9: A plot of all data found in Fig. 7. The data has been corrected by removing gravity in a manner consistent with Eq. (15). The line is the function given by Eq. (12).

Since Bond number is a function of the radius squared (see Eqs. (10)), we expect that the effective radius of curvature, R_{eff}, will scale as $\mathrm{Bo}^{1/2}$. Denoting the reference condition as Bo^*, we write

$$R_{eff} = R\left(\frac{\mathrm{Bo}}{\mathrm{Bo}^*}\right)^{1/2}, \qquad (14)$$

where R is the tube's radius. This new scaling is used to modify one of the radius terms in Eq. (12). Multiplying the leading radius term in $\zeta = R_2\left(1/R_2 - 1/R_1\right)$ by the correction allows us to write the free capillary flow scaling law with the addition of gravity as

$$\Pi\left(\frac{\mathrm{Bo}^*}{\mathrm{Bo}_2}\right)^{1/2} = \frac{1}{8}\xi^{-1}, \qquad (15)$$

where the subscript 2 denotes a quantity taken at the leading meniscus.

The data found in Fig. 7 has been adjusted by multiplying the experimental values of Π by $\left(\mathrm{Bo}_2/\mathrm{Bo}^*\right)^{1/2}$, thus *removing*, to first order, the effect of gravity from the data. These data are replotted in Fig. 9. We see that our prescription to remove gravity from the data causes it to become more closely aligned, in general, with the 1-D, gravity-free theoretical fluid model (Eq. (12)), plotted as a line in Fig. 9.

V. CONCLUSIONS

A one-dimensional fluid model of passive fluid flow in a capillary tube was developed. From the model, two non-dimensional similarity parameters, accounting for different fluid types and geometric combinations, were derived. The model was then tested using various fluids and several combinations of larger and smaller diameter capillary tubes. Applying the non-dimensional scaling to the dimensional data caused a collapse of the data from four orders of magnitude to within an order of magnitude of the one-dimensional model for almost every combination of tube radii. An additional, first-order gravitational correction allowed the data to be further collapsed by removing, to first-order, the effect of gravity. These data match, relatively well, the one-dimensional fluid model. This agreement strongly suggests the importance of the derived similarity parameters.

The attained physical insight provides us with the fundamental scaling laws to design a passive capillary feeding system for micropropulsion applications.

Acknowledgments

We gratefully acknowledge several helpful discussions with Dr. A. Darhuber and Dr. P. Felton.

[1] Terrestrial Planet Finder Science Working Group, *Terrestrial Planet Finder*, edited by C.A. Beichman, N.J. Woolf and C.A. Lindensmith, NASA Jet Propulsion Lab., JPL Publ. 99-003, California Inst. of Technology, Pasadena, CA, 1999.

[2] LISA Science Working Group, *LISA Mission Concept Study: Laser Interferometer Space Antenna for the Detection and Observation of Gravitational Waves*, edited by W.M. Folkner, P.L. Bender and R.T. Stebbins, NASA Jet Propulsion Lab., JPL Publ. 97-16, California Inst. of Technology, Pasadena, CA, 1997.

[3] Mueller, J., "Thruster options for microspacecraft: A review and evaluation of state-of-the-art and emerging technologies," *Micropropulsion for Small Spacecraft*, edited by M.M. Micci and A.D. Ketsdever, Vol. 187, Progress in Aeronautics and Astronautics, AIAA, Reston, VA, 2000, pp. 45-137.

[4] Mueller, J., "Review and applicability assessment of MEMS-based microvalve technologies for microspacecraft propulsion," In *Micropropulsion for Small Spacecraft*, edited by M.M. Micci and A.D. Ketsdever, Vol. 187, Progress in Aeronautics and Astronautics, AIAA, Reston, VA, 2000, pp. 449-476.

[5] Allen, R.R., Meyer, J.D., and Knight, W.R., "Thermodynamics and hydrodynamics of thermal ink jets," *Hewlett-Packard Journal*, Vol. 36, May 1985, pp. 21-27.

[6] Shoji, S. and Esashi, M., "Microflow devices and systems," *Journal of Micromechanics and Microengineering*, Vol. 4, No. 4, Dec. 1994, pp. 157-171.

[7] Elwenspoek, M., Lammerink, T.S.J., Miyake, R., and Fluitman, J.H.J., "Towards integrated microliquid handling systems," *Journal of Micromechanics and Microengineering*, Vol. 4, No. 4, Dec. 1994, pp. 227-245.

[8] West, G.D., "On the resistance to the motion of a thread of Mercury in a glass tube," *Proceedings of the Royal Society of London*, Vol. 86A, Issue 583, Dec. 22, 1911, pp. 20-25.

[9] Hoffman, R.L., "A study of the advancing interface: I. Interface shape in liquid-gas system," *Journal of Colloid and Interface Science*, Vol. 50, No. 2, Feb. 1975, pp. 228-241.

[10] Ward, C.A. and Sasges, M.R., "Effect of gravity on contact angle: A theoretical investigation," *Journal of Chemical Physics*, Vol. 109, No. 9, Sept. 1, 1998, pp. 3651-3660.

[11] Sasges, M.R. and Ward, C.A., "Effect of gravity on contact angle: An experimental investigation," *Journal of Chemical Physics*, Vol. 109, No. 9, Sept. 1, 1998, pp. 3661-3670.

[12] Cox, R.G., "Inertial and viscous effects on dynamic contact angles," *Journal of Fluid Mechanics*, Vol. 357, 1998, pp. 249-278.

[13] Darhuber, A.A., Troian, S.M., and Reisner, W.W., "Dynamics of capillary spreading along hydrophilic microstrips," *Physical Review E*, Vol. 64, 031603, 2002.

[14] Zengerle, R. and Richter, M., "Simulation of microfluid systems," *Journal of Micromechanics and Microengineering*, Vol. 4, No. 4, Dec. 1994, pp. 192-204.

[15] Jen, C.-P. and Lin, Y.-C., "Design and simulation of bi-directional microfluid driving systems," *Journal of Micromechanics and Microengineering*, Vol. 12, No. 2, Mar. 2002, pp. 115-121.

[16] Giordano, N. and Cheng, J.-T., "Microfluid mechanics: progress and opportunities," *Journal of Physics: Condensed Matter*, Vol. 13, No. 15, Apr. 16, 2001, pp. R271-R295.

[17] Ivanov, D. and Petrova, H., "Capillary effects," *Physics Education*, Vol. 35, No. 4, July 2000, pp. 262-266.

[18] Jahn, R.G. and Choueiri, E.Y., "Electric propulsion," *Encyclopedia of Physical Science and Technology*, 3^{rd} edition, Vol. 5, pages 125-141, Academic Press, San Diego, CA, 2002.

[19] Landau, L.D. and Lifshitz, E.M. *Fluid Mechanics*, Pergamon Press, London, 1959.

[20] Poynton, C.A., "A tutorial on magic numbers for high definition elecronic production," *Proceedings of the* 132^{nd} *SMPTE Technical Conference*, New York, Society of Motion Picture and Television Engineers, Oct. 13-17, 1990.

[21] *CRC Handbook of Chemistry and Physics*, 77^{th} edition, CRC Press, Inc., Boca Raton, FL, 1996.

[22] Sigma-Aldrich Corp., St. Louis, MO, 2002.

[23] Inland Vacuum Industries, Churchville, NY, 2002.

[24] Lamb, H. *Hydrodynamics*, Cambridge University Press, Cambridge, UK, 1932.